Local density of states of electron-crystal phases in graphene in the quantum Hall regime

O. Poplavskyy,[1,2,3,*] M. O. Goerbig,[2] and C. Morais Smith[3]
[1]*Faculty of Mathematics, University of Cambridge, Wilberforce Road, Cambridge CB3 0WA, United Kingdom*
[2]*Laboratoire de Physique des Solides, CNRS UMR 8502, Université Paris Sud, F-91405 Orsay Cedex, France*
[3]*Institute for Theoretical Physics, University of Utrecht, Leuvenlaan 4, 3584 CE Utrecht, The Netherlands*
(Received 16 February 2009; revised manuscript received 3 September 2009; published 17 November 2009)

We calculate, within a self-consistent Hartree-Fock approximation, the local density of states for different electron crystals in graphene subject to a strong magnetic field. We investigate both the Wigner crystal and bubble crystals with M_e electrons per lattice site. The total density of states consists of several pronounced peaks, the number of which in the negative energy range coincides with the number of electrons M_e per lattice site, as for the case of electron-solid phases in the conventional two-dimensional electron gas. Analyzing the local density of states at the peak energies, we find particular scaling properties of the density patterns if one fixes the ratio ν_N/M_e between the filling factor ν_N of the last partially filled Landau level and the number of electrons per bubble. Although the total density profile depends explicitly on M_e, the local density of states of the lowest peaks turns out to be identical regardless the number of electrons M_e. Whereas these electron-solid phases are reminiscent of those expected in the conventional two-dimensional electron gas in GaAs heterostructures in the quantum Hall regime, the local density of states and the scaling relations we highlight in this paper may be, in graphene, directly measured by spectroscopic means, such as, e.g., scanning tunneling microscopy.

DOI: 10.1103/PhysRevB.80.195414 PACS number(s): 73.43.−f, 73.20.Qt, 73.21.−b, 68.37.−d

I. INTRODUCTION

As was shown by Wigner in 1934,[1] the degenerate Fermi gas is unstable toward the formation of a periodic triangular lattice of localized electrons (electron crystal), once the Coulomb energy prevails over the kinetic one. Whereas a Wigner crystal (WC) has been observed at low electronic densities on the surface of liquid helium,[2] the critical electron density at which the transition to the WC occurs is too low for usual metals. Nevertheless, the situation is much improved if one applies a strong perpendicular magnetic field to a two-dimensional (2D) electron gas (2DEG). In this case, the single-particle continuous energy spectrum is quantized into a sequence of hugely degenerate Landau levels (LLs). If one restricts oneself to the electrons within the last partially filled LL, one finds that their kinetic energy is quenched, and the only energy scale is the Coulomb energy, which favors the formation of an electron crystal at small filling factors.[3–5]

A quantum electron crystal in the presence of a disorder potential is expected to become collectively pinned and to manifest itself as an insulator.[6] While at small filling factors the 2D WC with triangular lattice symmetry[4,5] is expected to yield the global energy minimum, it was predicted that the phase diagram of the 2DEG includes also electron-bubble crystals (a periodic lattice with more than one electron per site), stripes,[7–9] and even more exotic quantum Hall liquid-crystal phases.[10] Unlike electron-crystal phases, the prominent quantum liquids, which display the fractional quantum Hall effect in the two lowest LLs,[11] are translationally and rotationally invariant and remain conducting even in the presence of disorder. Therefore, these different quantum phases may be distinguished experimentally with respect to the behavior in transport measurements. For instance, a succession of insulating and conducting phases yields a re-entrant integer quantum Hall effect (IQHE) in the first[12] ($N=1$) and second[13] ($N=2$) excited LLs and has been interpreted in terms of a competition of such electron-solid and quantum-liquid phases.[14] Further evidence, prior to the above-mentioned transport measurements, for electron crystals in LLs stems from radio-frequency spectroscopy,[15,16] threshold behavior in the conductivity due to crystal pinning,[17] and more recent transport measurements under microwave irradiation,[18–22] which excites the collective pinning mode of the electron crystals.

While all these experimental techniques have been very successful in discovering unusual insulating phases and have confirmed a number of theoretical predictions, they are indirect evidence for high-field electron crystals based on transport measurements—the 2DEG in GaAs heterostructures is buried deep inside the substrate, which renders impossible a direct optical observation of a periodic electron-crystal lattice, e.g., by means of scanning tunneling microscopy (STM).[23] In contrast to the conventional 2DEG, such optical studies might become possible in graphene, a one-atom-thick sheet of graphite, with unique electronic and mechanical properties.[24,25] Indeed, graphene may be viewed as a particular 2DEG, where the electrons behave as if they were massless particles described by the relativistic 2D Dirac equation. In this Dirac equation, the Fermi velocity v_F plays the role of the speed of light c, although it is roughly 300 times smaller than the latter in vacuum. In addition, the Brillouin zone of graphene has two nonequivalent corner points (called Dirac points), which yield a twofold valley degeneracy and which may formally be described in terms of an SU(2) pseudospin degree of freedom.

In strong magnetic fields, the energy of Dirac fermions in graphene is quantized into LLs, the structure of which is different from that of nonrelativistic electrons in a conventional 2DEG. Apart from their unconventional (square root) magnetic-field dependence, there exists a LL at exactly zero

energy, and each LL in the conduction band has a counterpart in the valence band. This particular LL structure leads to the anomalous integral quantum Hall effect observed in graphene.[26,27] In addition, the energy gap between the subsequent LL's in graphene is so large, that it is possible to observe the IQHE even at room temperatures.[28]

As the mobility of graphene samples is further improved, one may expect to observe the fractional quantum Hall effect, which has been studied theoretically by several authors,[29–34] and also collectively pinned insulating phases, such as Wigner-crystal and bubble phases, as predicted in Refs. 35–39. In contrast to GaAs heterostructures, these electronic phases occur at the surface of the graphene sheet and are, thus, directly accessible by spectroscopic means. Indeed STM has been applied successfully to probe the density distribution in exfoliated[40] and epitaxial[41] graphene, as well as in graphene on a graphite substrate in a strong magnetic field.[42] This exciting prospect motivated us to calculate theoretically physical quantities of a 2D electron crystal which might be measured in an STM experiment: the (integrated) density of states (DOS) and the local DOS (LDOS). We should note that the quantum Hall regime is the only case for which one may expect the formation of electron-crystal phases in graphene. Indeed, it is predicted that the 2D Wigner crystallization is completely absent in graphene for any electron density in the absence of a magnetic field,[43] due to the scale invariance of the dimensionless interaction parameter $r_s = e^2/\hbar\epsilon v_F \simeq 2/\epsilon$ for a 2D system with a linear dispersion relation. Here, ϵ is the dielectric constant which depends on the environment where the graphene sheet is embedded.

In this paper, we discuss the DOS and the LDOS for several electron crystals in the $N=2$ LL within a Hartree-Fock approximation. We have performed similar calculations for $N=0$, 1, 3, and 4, but we concentrate in the present paper on $N=2$ for two reasons. First, the DOS and LDOS results for $N=2$ are representative of high-field electron solids—our calculations yield indeed similar results for the other LLs. Second, for higher LLs there have been no clear indications so far for electron-crystal phases in GaAs in the quantum Hall regime. For our numerical calculations, we have adopted the iterative scheme proposed by Côté and MacDonald,[44,45] which has also been applied to calculate the energies and the real-space profiles of various electron-crystal phases in graphene.[35] As a test of the validity of our code, we have corroborated the results obtained in Ref. 35 and then applied it for the calculation of the DOS and the LDOS. Notice that, despite the huge amount of Hartree-Fock studies of quantum Hall electron-crystal phases, none is devoted to study the LDOS of these phases. We have calculated the LDOS at energies where the integrated DOS has well-pronounced peaks, which fall into two distinct classes: bound states at negative energy with respect to the chemical potential and high-energy peaks above. The number of negative-energy peaks is identical with the number of electrons M_e per bubble, in agreement with bubble crystals in the conventional 2DEG.[9] Furthermore, we find that the sum of the LDOS at these M_e negative-energy peaks reproduces the real-space density profile of the M_e-electron bubble crystal.

This paper is organized as follows. In Sec. II, we outline the basic steps of the Hartree-Fock approximation to the 2DEG in graphene. In Sec. III, we present numerical results for the DOS and the LDOS in graphene, and we briefly discuss our results for $N=0$ in Sec. IV. Finally, we draw our conclusions in Sec. V.

II. HARTREE-FOCK HAMILTONIAN

For a partially filled LL N, the low-energy electronic properties are captured within a model that takes into account states only within this level. In this case, the single-particle kinetic energy is the same for all of states, and thus only the interaction term is relevant. Furthermore, we omit the physical spin, which we consider to be completely polarized, e.g., due to a sufficiently large Zeeman effect. The derivation of the Hartree-Fock Hamiltonian for the 2DEG in GaAs has been extensively discussed in the literature.[44,45] In graphene, the interaction Hamiltonian for the 2DEG is similar to that in GaAs, albeit with different form factors due to the spinorial form of the wave functions.[29,46] This similarity allows one to use the same theoretical methods which were used previously to study the 2DEG in GaAs, with the important difference that we need to take into account the twofold valley degeneracy in the form of an SU(2) pseudospin degree of freedom, $\beta = \pm 1$. Provided that inter-LL transitions are neglected, we may write the interaction part of the full Hamiltonian for the 2DEG of spinless electrons in graphene as[29]

$$\hat{\mathcal{H}}_{\rm int} = \frac{V_{\rm C}}{2} \sum_{\beta,\beta',\mathbf{q}} \frac{1}{|\mathbf{q}|} [\mathcal{F}_N(\mathbf{q})]^2 \hat{\rho}_{\beta,\beta}(-\mathbf{q}) \hat{\rho}_{\beta',\beta'}(\mathbf{q}), \tag{1}$$

where $V_{\rm C} \equiv e^2/l_B\epsilon$ is the Coulomb energy scale, with $l_B = \sqrt{\hbar/eB}$ the magnetic length, B is the magnetic field, and ϵ is the dielectric susceptibility of the medium and $\mathbf{q} \equiv (q_x, q_y)$ is a 2D wave vector. The (guiding center) density operator in the Landau gauge reads

$$\hat{\rho}_{\beta_1,\beta_2}(\mathbf{q}) = N_\phi^{-1} \sum_X \exp\left(-iq_xX - i\frac{l_B^2 q_x q_y}{2}\right) \times \hat{c}^\dagger_{X,\beta_1} \hat{c}_{X+l_B^2 q_y,\beta_2}. \tag{2}$$

Here, $N_\phi = S/2\pi l_B^2$ measures the LL degeneracy, with the square area S of the 2DEG sample, $\hat{c}_{X,\beta}$ and $\hat{c}^\dagger_{X,\beta}$ are the electron's destruction and creation operators, respectively, where X denotes single-particle quantum states within the Nth LL. Finally, in Eq. (1) the graphene form factor $\mathcal{F}_N(\mathbf{q})$ reads[29,46]

$$\mathcal{F}_N(\mathbf{q}) = \begin{cases} \frac{1}{2}\left[L_{|N|}\left(\frac{q^2 l_B^2}{2}\right) + L_{|N|-1}\left(\frac{q^2 l_B^2}{2}\right)\right] e^{-q^2 l_B^2/4}, & N \neq 0; \\ e^{-q^2 l_B^2/4}, & N = 0, \end{cases} \tag{3}$$

where $q \equiv |\mathbf{q}|$ and $L_n(x)$ is the Laguerre polynomial of order n. We note that the 2DEG form factor in GaAs is given by[44]

$$F_N(\mathbf{q}) = L_N\left(\frac{q^2 l_B^2}{2}\right) e^{-q^2 l_B^2/4}. \tag{4}$$

It is apparent from Eqs. (3) and (4) that the graphene (relativistic 2DEG) form factor is simply a linear combination of

form factors for adjacent LLs of the nonrelativistic 2DEG in GaAs. This peculiar fact results from mixing the Dirac particle wave functions between the sites of two sublattices in graphene, and is also a consequence of the spinorial nature of these wave functions. Apart from the difference in form factors given by Eqs. (3) and (4), the 2DEG in GaAs and graphene is described equivalently, as follows from the same analytical structure of the Coulomb interaction term given by Eq. (1).

Finally, we note that the Hamiltonian in Eq. (1) is SU(2) invariant with respect to the valley pseudospin. In contrast to the physical electron spin, this SU(2) symmetry is approximate. However, SU(2)-symmetry-breaking terms are suppressed linearly in $a/l_B \ll 1$ where $a=0.14$ nm is the carbon-carbon distance in graphene and $l_B=26/\sqrt{B[\mathrm{T}]}$ nm, i.e., at an energy scale that is well below the disorder broadening of the LL's.[29,47] This physical model is similar to another two-component quantum Hall system—if one replaces in Eq. (1) $\mathcal{F}_N(\mathbf{q})$ by the nonrelativistic form-factor $F_N(\mathbf{q})$, one obtains the Hamiltonian for the nonrelativistic 2DEG including the electrons' spin in the absence of a polarizing Zeeman effect. Alternatively, this model may describe a quantum Hall bilayer in the theoretical limit of zero layer separation, where the two "spin" orientations denote the two different layers.[45] One may further simplify the model in Eq. (1) by omitting the valley pseudospin degree of freedom, in which case one presupposes a complete valley polarization of the electronic phases, which would maximally profit from the exchange interaction. This effective U(1) model is described by the interaction term

$$\hat{\mathcal{H}}_{\mathrm{int}} = \frac{V_C}{2}\sum_{\mathbf{q}} \frac{1}{|\mathbf{q}|}[\mathcal{F}_N(\mathbf{q})]^2 \hat{\rho}(-\mathbf{q})\hat{\rho}(\mathbf{q}), \tag{5}$$

where the density operator of spinless electrons $\hat{\rho}(\mathbf{q})$ is obtained from Eq. (2) by neglecting the pseudospin indices. This simplified U(1) model of fully valley-polarized graphene, which is described by Eq. (5), is called *U(1)-graphene* in the remainder of the paper. Now, if one substitutes into Eq. (5) the nonrelativistic form-factor $F_N(\mathbf{q})$, one obtains the usual single-layer quantum Hall 2DEG for spin-polarized electrons in GaAs.

The Hartree-Fock approximation applied to the graphene interaction term in Eq. (1) yields[35,45]

$$\hat{\mathcal{H}}_{\mathrm{int}}^{(\mathrm{HF})} = N_\phi V_C \sum_{\beta,\mathbf{Q}} \{[H(\mathbf{Q}) - X^{\beta\beta}(\mathbf{Q})]\hat{\rho}_{\beta,\beta}(\mathbf{Q}) - X^{\beta\bar{\beta}}(\mathbf{Q})\hat{\rho}_{\bar{\beta},\beta}(\mathbf{Q})\}, \tag{6}$$

where $\bar{\beta}=-\beta$ and $\mathbf{Q}$'s are the reciprocal wave vectors of the WC lattice. The Hartree and Fock effective interaction potentials read, respectively,

$$H(\mathbf{Q}) = \frac{e^{-Q^2 l_B^2/2}}{Q}|\mathcal{F}_N(\mathbf{Q})|^2 \rho(-\mathbf{Q})(1-\delta_{\mathbf{Q},0}), \tag{7}$$

$$X^{\beta\beta'}(\mathbf{Q}) = l_B \int_0^\infty dx e^{-x^2/2}|\mathcal{F}_N(x)|^2 J_0(xQl_B)\rho_{\beta,\beta'}(-\mathbf{Q}), \tag{8}$$

where $Q\equiv|\mathbf{Q}|$, J_0 is a Bessel function, and the density averages are $\rho_{\beta,\beta'}(\mathbf{Q})=\langle\hat{\rho}_{\beta,\beta'}\mathbf{Q}\rangle$ and $\rho(\mathbf{Q})=\Sigma_\beta\rho_{\beta,\beta}(\mathbf{Q})$. We assume a triangular electron lattice for the broken-symmetry state, with reciprocal lattice vectors given by

$$\mathbf{Q} = Q_0\left(\frac{n}{2}, \frac{n}{2}+\frac{m\sqrt{3}}{2}\right), \quad n,m \in \mathbb{Z}. \tag{9}$$

Here Q_0 is the length of the basis vector of the reciprocal lattice,

$$Q_0 = l_B^{-1}\left(\frac{4\pi\nu_N}{\sqrt{3}M_e}\right)^{1/2}, \tag{10}$$

where ν_N is the filling factor of the last partially filled LL and M_e is the number of electrons per site ($M_e=1$ corresponds to the WC and $M_e\geq 2$ to an electron-bubble crystal with M_e electrons per bubble). The single-particle Green's function in the imaginary-time Matsubara formalism[48] reads

$$G_{\beta_1,\beta_2}(\mathbf{Q},i\omega_n) = -N_\phi^{-1}\int_0^{\hbar/k_BT} d\tau \exp(i\omega_n\tau) \times \sum_X \exp\left[-iQ_xX + \frac{l_B^2 Q_x Q_y}{2}\right] \times \langle \mathcal{T}_\tau \hat{c}_{X-l_B^2Q_y,\beta_1}(\tau)\hat{c}^\dagger_{X,\beta_2}(0)\rangle, \tag{11}$$

where T is the temperature, k_B is the Boltzmann constant, $\mathcal{T}_\tau$ denotes imaginary-time ordering, and $\omega_n=\pi(2n+1)k_BT/\hbar$ are the Matsubara frequencies. $G_{\beta_1,\beta_2}(\mathbf{Q},i\omega_n)$ may be determined self-consistently from quadratic Hamiltonian (6) by using the Heisenberg equations of motion within the iterative-solution method proposed in Ref. 44, which we adopt in the present work.

After analytic continuation to real frequencies $i\omega_n\rightarrow\omega+i0^+$, $G_{\beta_1,\beta_2}(\mathbf{Q},i\omega_n)$ yields the retarded Green's function which may be used to calculate the DOS $g(\omega)$,

$$g(\omega) = -N_\phi^{-1}\pi\sum_\beta \mathrm{Im}\, G_{\beta,\beta}(\mathbf{Q}=0, i\omega_n\rightarrow\omega+i0^+) \tag{12}$$

and the LDOS $A(\mathbf{r},\omega)$,

$$A(\mathbf{r},\omega) = -N_\phi^{-1}\pi\sum_\beta \mathrm{Im}\, G_{\beta,\beta}(\mathbf{r}, i\omega_n\rightarrow\omega+i0^+), \tag{13}$$

where the Green's function in real space reads

$$G_{\beta_1,\beta_2}(\mathbf{r},i\omega_n) = (2\pi l_B^2)^{-1}\sum_{\mathbf{Q}} \exp(-i\mathbf{Q}\cdot\mathbf{r})\mathcal{F}_N(-\mathbf{Q}) \times G_{\beta_1,\beta_2}(\mathbf{Q},i\omega_n). \tag{14}$$

III. ELECTRON CRYSTALS IN $N=2$

In this section, we discuss the spectroscopic properties of the electron-solid phases for the LL $N=2$. As already mentioned in the introduction, we concentrate on this LL for

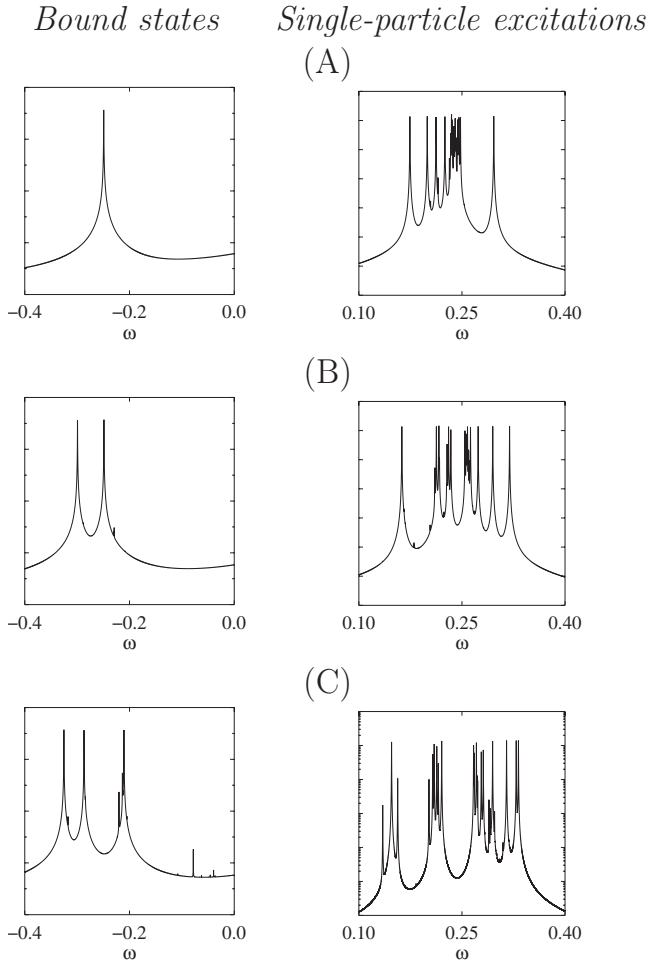

FIG. 1. Logarithmic plots for the density of states $g(\omega)$ of graphene in the $N=2$ Landau level at (A) $M_e=1$, $\nu_N=0.14$; (B) $M_e=2$, $\nu_N=0.28$; and (C) $M_e=3$, $\nu_N=0.42$. The frequency ω is given in units of the Coulomb scale V_C. The $\omega=0$ frequency is the position of the chemical potential (Fermi energy) μ. The infinitesimal imaginary frequency shift $\omega \to \omega + i0^+$ is approximated by $\omega \to \omega + i\delta_\omega$, with $\delta_\omega = 10^{-4}$. Figures (A)–(C) in the left column yield the DOS in the low-energy frequency range (bound states of electrons), while in the right column the high-energy peaks of the DOS correspond to single-electron excitations above the ground state of the lattice.

illustration purposes and because it is more significant than the other LLs from the physical point of view. We have obtained similar results for $N=3$ and 4 (not discussed here). The zero-energy LL ($N=0$) turns out to be quite particular and will be discussed briefly in Sec. IV.

We have chosen three different electron-solid lattices which have the same ratio $\nu_N/M_e = 0.14 \approx 1/7$, and hence the same lattice period given by Eq. (10). Our choice for the ν_N/M_e ratio is rather arbitrary. We note that the $M_e=1$ and 2 states yield in graphene the global energy minima, while the $M_e=3$ does not. It has been shown in Ref. 35 that the ground state of graphene at $\nu_N \leq 0.43$ is an anisotropic Wigner crystal whereas at $0.28 \leq \nu_N \leq 0.43$ the ground state is the $M_e=2$ bubble crystal, and at $\nu_N \leq 0.28$ the Wigner crystal yields the lowest energy ($M_e=1$). Therefore, the $M_e=3$ phase is not the lowest-energy state in graphene; nevertheless, it is useful to analyze on the same footing all three cases $M_e=1$, 2, and 3.

For completeness, we mention that we have also calculated the cohesive energies of other types of electron-crystal phases (not only triangular bubble phases but also anisotropic Wigner crystals). Our results for the energies coincide with those of Ref. 35 with excellent accuracy and, therefore, corroborate the DOS and LDOS results discussed below.

A. (Integrated) density of states

Our results for the DOS in graphene at $N=2$ are presented in Fig. 1. We find that the DOS consists of two well-separated classes of peaks: well-defined low-energy peaks are found below the chemical potential μ, which is shifted to zero energy, whereas the large number of peaks above μ are not that easily distinguished. We note here that in graphene the number of low-energy peaks in all cases is equal to M_e, the number of electrons in a bubble. The same result has been obtained before in Hartree-Fock studies of the simpler single-layer 2D quantum Hall system.[9] We checked that the same property holds true also for U(1)-graphene, and in nonrelativistic two-component quantum Hall systems, such as a bilayer with zero layer separation.

In the simpler single-layer 2D quantum Hall system in GaAs, the DOS at $M_e=1$ exhibits the features of the Hofstadter butterfly structure.[9] It means the following: given that the filling factor may be represented by a ratio of two integers p and q without a common divisor, $\nu_N = p/q$, these integers p and q determine then the structure of the single-particle energy spectrum of the system; namely, there should exist p low-energy levels and $q-p$ high-energy levels (Hofstadter butterfly counting rule). In the DOS, which is a function of frequency, these energy levels are recognized as smoothed peaks. The Hofstadter butterfly counting rule was confirmed for $M_e=1$ in the single-layer 2DEG in GaAs, while for $M_e \geq 2$ it is claimed that the counting of the single-particle levels is different: the number of low-energy peaks is equal to M_e, whereas nothing is known about what is the precise rule for counting the number of high-energy peaks.[9]

What will be important in the following discussion is the *order of indexing of the DOS peaks*. We will count the peaks in the DOS with respect to *increasing the frequency* ω. In Fig. 1(A), the *first* DOS peak is obviously the lowest-energy

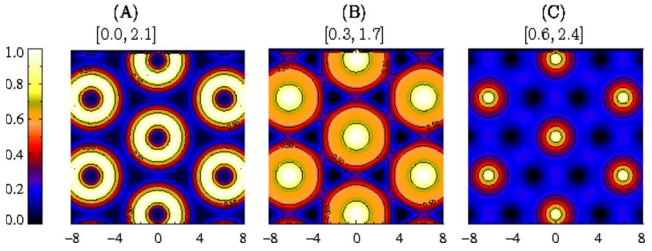

FIG. 2. (Color online) Real-space density profile $n(\mathbf{r})$ in graphene in the $N=2$ LL. Choices (A)–(C) are the same as in Fig. 1. Minima and maxima of $n(\mathbf{r})$ written inside the square brackets as [min, max] correspond to the values [0.0, 1.0] in the color plots (blue and white colors, correspondingly). The x and y axes are in units of l_B.

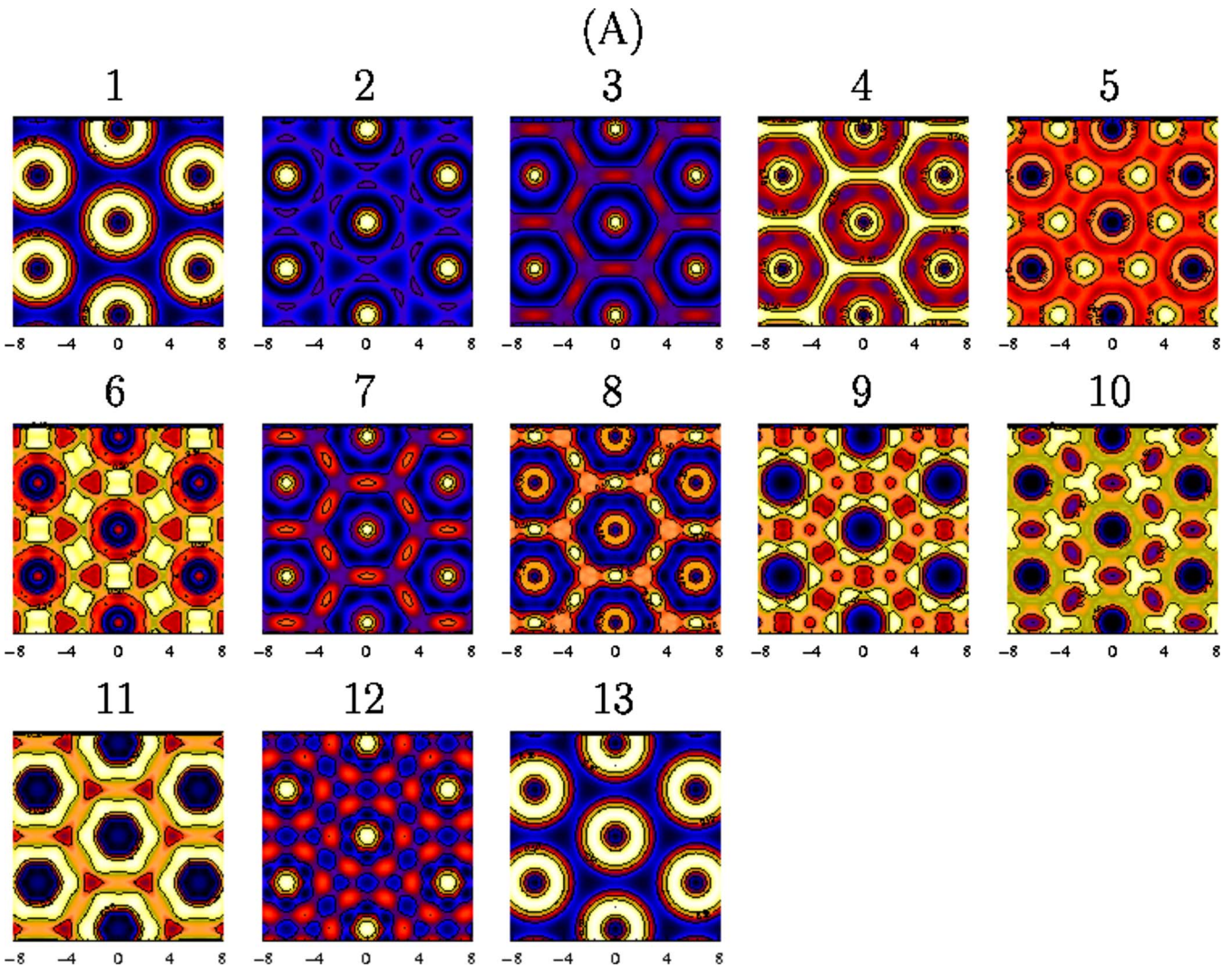

FIG. 3. (Color online) LDOS $A(\mathbf{r},\omega)$ for graphene at $\nu_N=0.14$, $M_e=1$ [case (A)]. Contour colors are graded in the same way as defined in Fig. 2. The contour plots are ordered with respect to the index of DOS peaks (indicated above the plots). The x and y axes are in units of l_B. The number of extracted DOS peaks is $N_p=13$.

one with energy $\approx -0.24V_C$. The *second peak* in (A) is a higher-energy one with energy $\approx 0.17V_C$. The numbering of peaks continues until we reach the utmost-right peak with energy $\approx 0.3V_C$. The same indexing rule is applied to the cases (B) and (C). One should note that in all three cases the DOS peaks with the same index may have rather different energies: while in (A) the second DOS peak belongs already to the high-energy region, in (B) it still lies below the Fermi level.

In addition, one should have a procedure of extracting the energies of the DOS peaks from the smoothed DOS vs frequency dependence shown in Fig. 1. In the low-energy regime it may be always done reliably. In the high-energy regime, however, there is a larger number of closely located DOS peaks, the shapes, widths, and amplitudes of which depend sensitively on the imaginary frequency shift δ_ω. The latter is used for the analytical continuation into the upper complex half-plane of the Green's function, $i\omega_n \to \omega + i\delta_\omega$. Physically, this imaginary frequency shift represents a level broadening, e.g., due to disorder. We have found that the best way to extract only those peaks which are physical is to place a cutoff Δ on the DOS peak amplitude, so that peaks with amplitude less than $g_{\max}\Delta$ are neglected, with $g_{\max} \propto \delta_\omega^{-1}$ the maximum peak amplitude. In our study, we have chosen $\delta_\omega = 10^{-4}$ and $\Delta = 0.5$. The number of shells of reciprocal lattice vectors $\mathbf{Q}$'s is $N_{sh}=8$, so that the actual number of vectors is $N_Q=241$. Single-particle energies which are extracted from the smoothed DOS, will be used below in the calculation of the LDOS. In the U(1)-graphene and the single-layer cases at the same densities considered here, we are able to extract seven DOS peaks; at $\nu_N=0.14$ and $M_e=1$, there is one lowest-energy peak and six high-energy ones. These are exactly the numbers of single-particle levels dictated by the Hofstadter butterfly counting rule.[9]

In graphene and the quantum Hall bilayer, studied within the two-component model, we obtain the number of identified DOS peaks around 14 (with deviation of not more than one wrongly identified peak). Due to the additional SU(2) symmetry in the latter two cases, it is natural to expect that the number of single-particle levels is thus *doubled*.

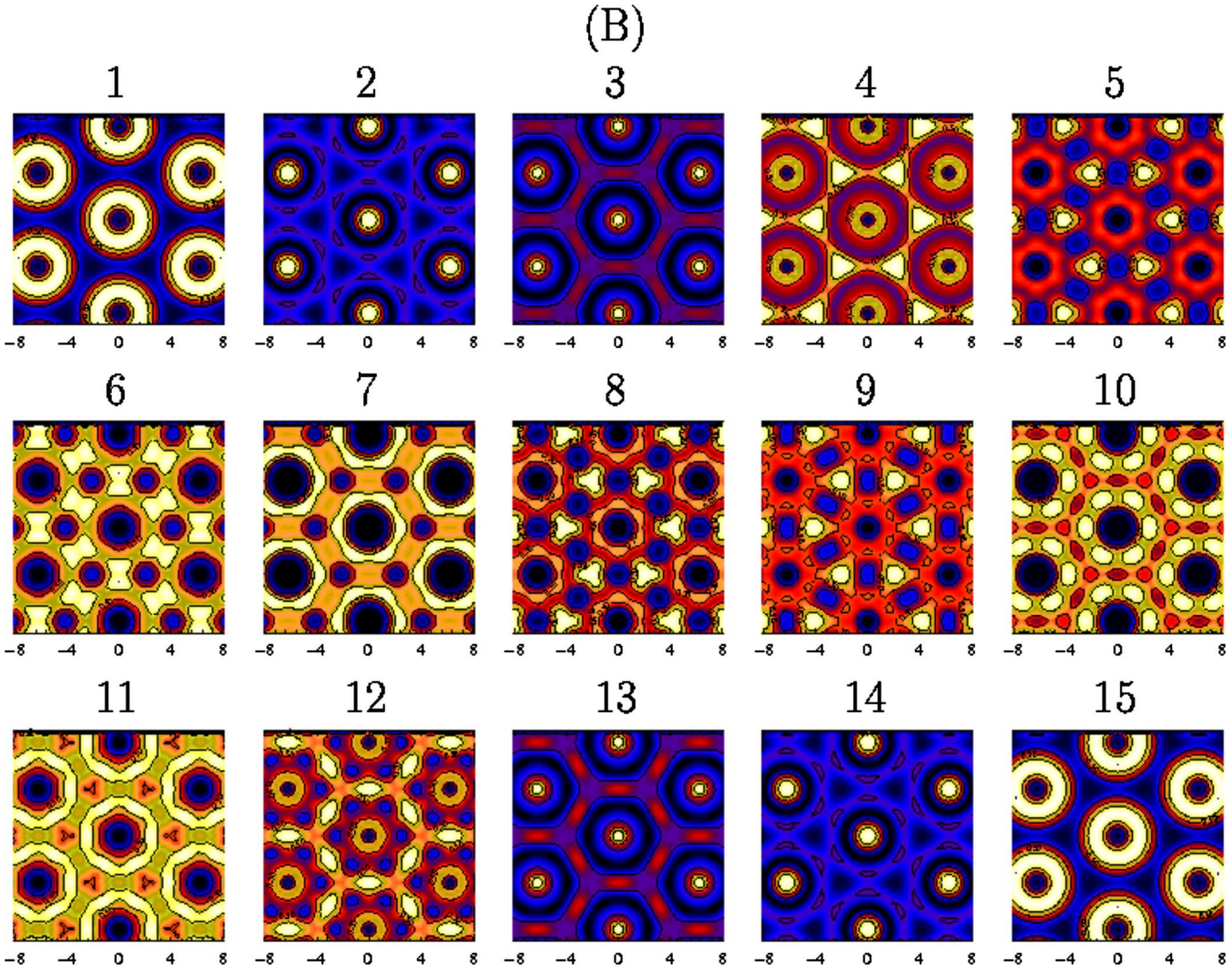

FIG. 4. (Color online) LDOS $A(\mathbf{r},\omega)$ for graphene at $\nu_N=0.28$, $M_e=2$ [case (B)]. The x and y axes are in units of l_B, $N_p=15$.

B. Real-space density profile

For later comparison with our results for the LDOS, we calculated the real-space electron-density profile

$$n(\mathbf{r}) = \frac{1}{2\pi l_B^2} \sum_{\mathbf{Q}} \exp(-i\mathbf{Q}\cdot\mathbf{r}) \mathcal{F}_N(-\mathbf{Q}) \rho(\mathbf{Q}) \qquad (15)$$

for the same choices of (ν_N, M_e) as in Fig. 1. The results, which are shown in Fig. 2, agree with previous calculations for graphene performed by Zhang and Joglekar.[35]

C. Local density of states

Our results for the LDOS in graphene are presented in Figs. 3–5. The LDOS patterns are plotted for all three cases (A)–(C), as in Fig. 1 and at the energies of all extracted single-particle DOS peaks situated in increasing order. We obtain that the *rescaled*, to the range of [0.0, 1.0], real-space patterns of $A(\mathbf{r},\omega)$, calculated at the *first four* DOS peaks for all three choices of (ν_N, M_e), coincide among themselves. There is also an approximate mapping between the LDOS patterns at the fifth DOS peak, although less pronounced than for the first four ones (one sees correspondence between the positions of maxima and minima, but the colors deviate slightly in each case). For larger values of the peak index, we start to see considerable discrepancies between the LDOS patterns. Also the number of extracted peaks N_p is different for each case. The latter property is due to the very approximate nature of our extraction procedure: while low-energy peaks are always identified reliably, the high-energy peaks are determined only approximately. However, the accuracy is quite good.

As for a possible explanation of the observed coincidence between the LDOS at the first energy peaks with different choices of (ν_N, M_e), one notices two aspects. First, the lattice constant is chosen to be the same for all three cases $M_e=1$, 2, and 3, as already mentioned above. Second, one may interpret the jth peak in the integrated DOS as the energy of the quasiparticle excitation on lattice sites that contain already $j-1$ electrons. Whereas the associated density pattern, revealed by the LDOS at the given energy, is then the same for all values of M_e, the quasiparticle excitation naturally corresponds to a bound state only if $j \leq M_e$.

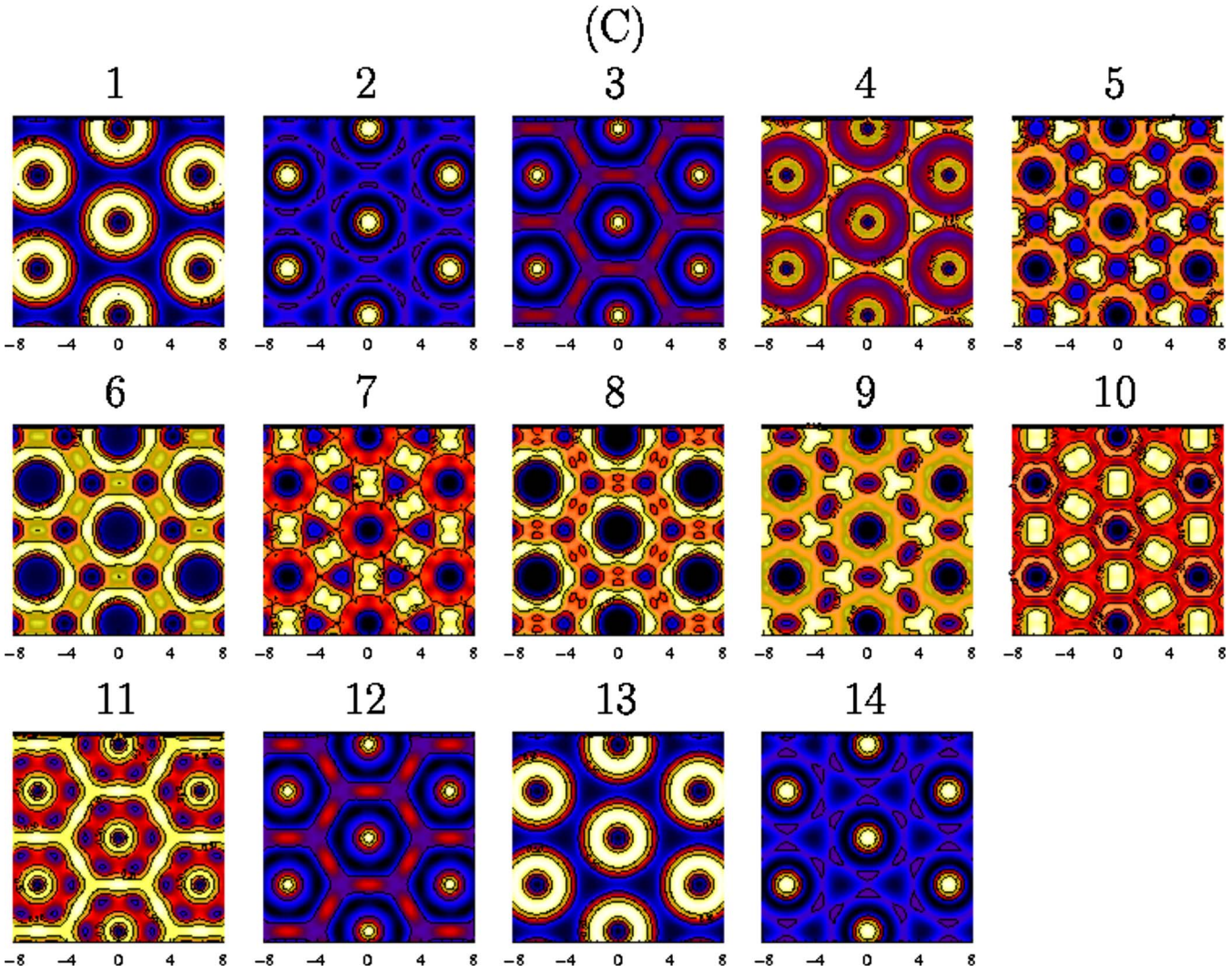

FIG. 5. (Color online) LDOS $A(\mathbf{r},\omega)$ for graphene at $\nu_N=0.42$, $M_e=3$ [case (C)]. The x and y axes are in units of l_B, $N_p=14$.

We also note a very interesting property of the LDOS at the last two peaks for (B) and (C): the LDOS patterns are identical, but their positions are *swapped*. We do not have any physical argument why this should be the case, but it could be a feature that appears when $M_e > N$. However, this statement is a mere speculation and a more detailed investigation is required to clarify this aspect.

D. Comparison with the real-space density

Now, to compare the LDOS patterns shown in Figs. 3–5 with the real-space density profile $n(\mathbf{r})$ defined in Eq. (15) and plotted in Fig. 2, we introduce the *resummed* LDOS $\tilde{A}(\mathbf{r},\omega)$, defined for a fixed single-particle energy ω_i as a sum of all LDOS patterns at smaller peak energies,

$$\tilde{A}(\mathbf{r},\omega_i) = \sum_{j=1}^{i} A(\mathbf{r},\omega_j). \tag{16}$$

Given the excellent coincidence of the LDOS patterns shown in Fig. 6 with the real-space densities in Fig. 2, one may empirically write

$$n(\mathbf{r}, M_e = i) \leftrightarrow \tilde{A}(\mathbf{r},\omega_i), \quad i = 1,2,3, \tag{17}$$

where the sign $\leftrightarrow$ means mapping between the *rescaled to the [0.0, 1.0] interval* quantities. This means that the real-space density of the M_e-electron bubble crystal is determined by the sum of the LDOS at the M_e negative-energy peaks. More surprisingly, because of the correspondence between the LDOS patterns of the low-energy peaks for all different M_e bubble crystals, one may determine the real-space density

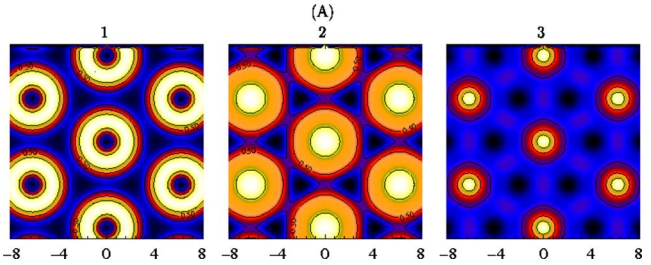

FIG. 6. (Color online) Resummed LDOS $\tilde{A}(\mathbf{r},\omega)$ for graphene at the three first DOS peaks for (A) [$\nu_N=0.14$, $M_e=1$]. Contour colors are graded in the same way as defined in Fig. 2.

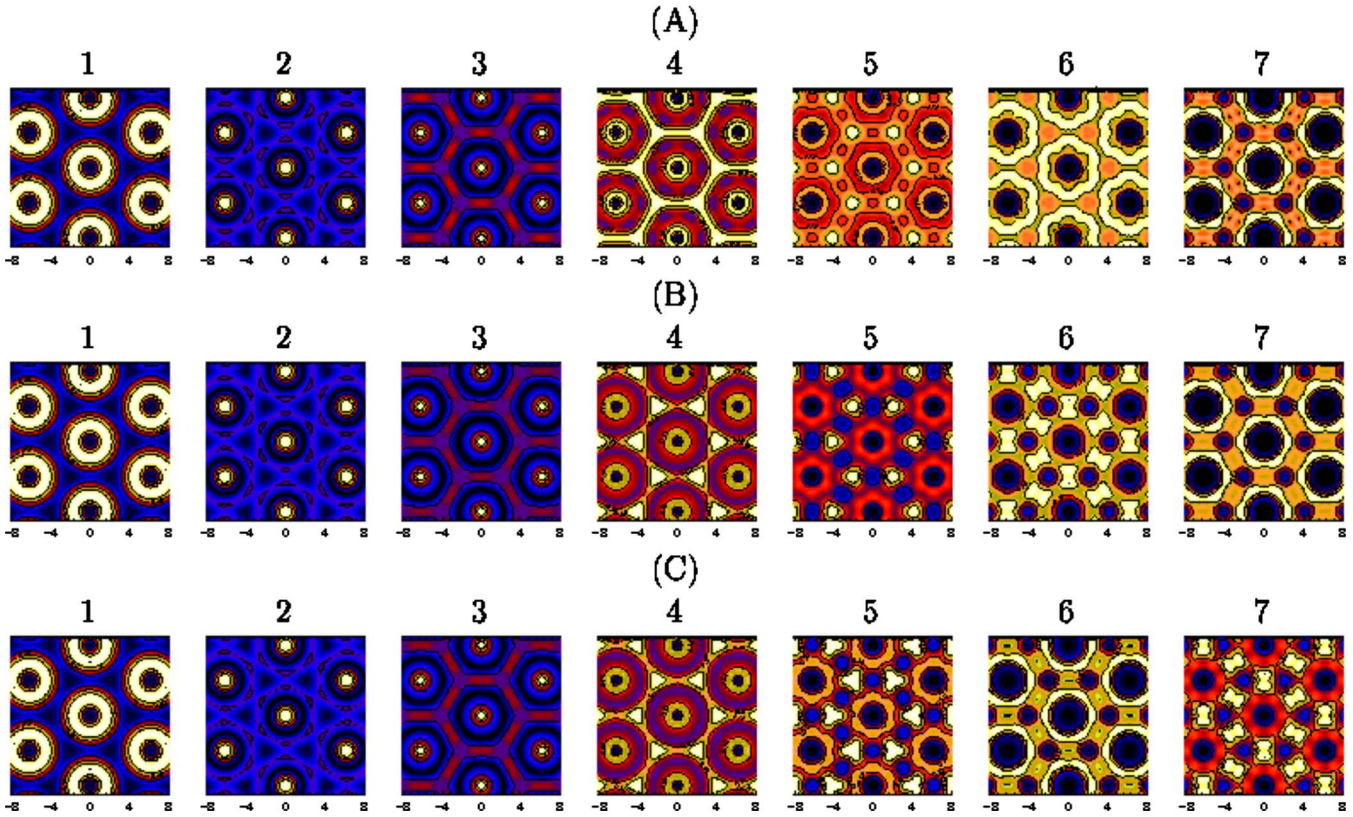

FIG. 7. (Color online) LDOS $A(\mathbf{r},\omega)$ for U(1)-graphene. The x and y axes are in units of l_B. The number of extracted DOS peaks $N_p=7$.

pattern of the M_e bubble crystal by summing the LDOS of the M_e peaks of lowest energy for *any* of the electron-solid phases—the LDOS patterns of the $M_e=1$ Wigner crystal, e.g., contains thus the information of the density of all other M_e bubble crystals.

E. U(1)-graphene: Local density of states

In Fig. 7, we present the LDOS for U(1)-graphene. The number of extracted DOS peaks for all three density choices (A), (B), and (C) is $N_p=7$. This is in accordance with the Hofstadter butterfly counting rule. We also see an excellent correspondence of the LDOS for the first four DOS peaks, then, also a good coincidence of the LDOS at the peaks six and seven for (A) and (B), whereas these two LDOS patterns for (C) interchange places, as compared with the patterns six and seven for (A) and (B). This interchange phenomenon is the same as observed for graphene and is not yet understood.

In general, the U(1)-graphene results coincide numerically with those for graphene when one takes into account the SU(2) symmetry for the valley pseudospin. This indicates that one may use the U(1) model instead of the more complex SU(2) symmetric one for the discussion of the density patterns, hence simplifying further calculations on graphene. Moreover, it indicates that in the electron-crystal phases considered above the valley degree of freedom is fully polarized.

IV. WIGNER CRYSTAL IN $N=0$

In the past section, we have concentrated on electron-crystal phases in higher LLs ($N\geq 2$) because of the particular competition between crystals with different electron number M_e per site. The LLs $N=0$ and 1 are different, and we briefly discuss the zero-energy LL $N=0$ here. Notice that in both levels $N=0$ and 1 only one type of electron crystal is present, namely, the $M_e=1$ WC.[35] As for the usual 2DEG, the WC turns out to compete with possible incompressible quantum liquid phases that display the fractional quantum Hall effect,[34] and the WC is then expected to occur at low values of the filling factor.

The density profile for the WC in $N=0$ is shown in the left panel of Fig. 8 for a partial filling factor of $\nu_N=0.14$. Although no variational studies comparing the energies for the WC and incompressible quantum liquids in graphene have, to the best of our knowledge, been performed, one may

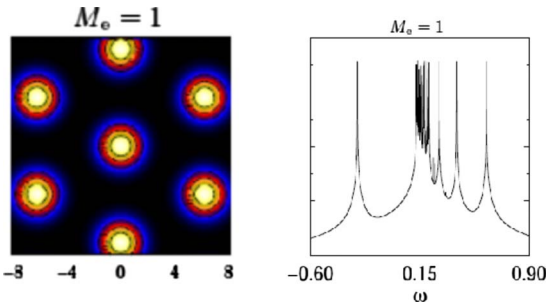

FIG. 8. (Color online) Left: real-space density profile $n(\mathbf{r})$ for the WC in the zero-energy LL $N=0$ at $\nu=0.14$. Right: logarithmic plot for the density of stats $g(\omega)$ of the $N=0$ WC at $\nu=0.14$. The frequency is measured in units of V_C.

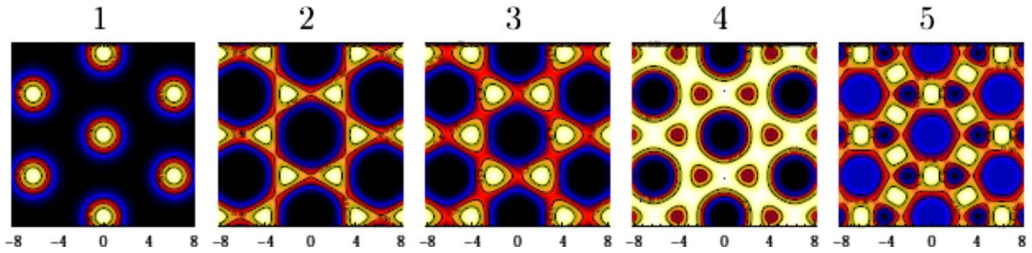

FIG. 9. (Color online) LDOS $A(\mathbf{r},\omega)$ at the lowest five peaks of the DOS for the WC in $N=0$ at $\nu=0.14$.

speculate that the ground state at $\nu_N=0.14$ in $N=0$, as well as in $N=1$, is indeed given by a WC. This is corroborated, on the one hand, by the fact that the $N=0$ LL in graphene is equivalent to that in the usual 2DEG, where the ground state is a WC,[49] and, on the other hand, by the strong similarity between the interaction potentials in the $N=0$ and 1 graphene LL.[29]

One notices that the real-space density profile of the WC in $N=0$ (Fig. 8) is remarkably different from that in higher LLs [Fig. 2(A)]—instead of a ringlike shape of the electronic density around the lattice sites, one obtains a density that is similar to a filled circle. This difference may be explained by the different nature of the one-particle wave functions in $N=0$ as compared to higher LLs. Indeed, the wave function in the lowest LL is a simple Gaussian with no node structure, whereas the probability density of a semiclassical state in higher LLs reflects the cyclotron motion, with a maximum at the cyclotron radius $R_C=l_B\sqrt{2N+1}$.

In Fig. 9 we show the LDOS patterns of the WC at the first five peaks in the DOS (right panel of Fig. 8) at $\nu=0.14$ for $N=0$, which may be accessible in an STM measurement. As in the case of higher LLs, the LDOS measured at the first (negative-energy) peak in the DOS has the same structure as the real-space density profile of the WC (left panel of Fig. 8). Remarkably, the scaling properties between the peaks, discussed in Sec. III C for $N=2$, are absent in $N=0$. This absence may be due to the different shape of the one-particle wave functions—remember that these wave functions are Gaussian in $N=0$, whereas they are of ringlike shape in higher LLs, as mentioned above. Notice furthermore, that the positive-energy peaks in the DOS for the WC are much denser in $N=0$ (right panel of Fig. 8) than in $N=2$ [see Fig. 1(A), right panel]. This is also the case for the DOS of bubble crystals (unphysical in $N=0$) with $M_e>1$ (figures not shown). It is therefore more delicate to index the high-energy peaks in $N=0$; hence, one may not safely conclude about the presence or the absence of scaling properties in $N=0$.

V. CONCLUSIONS

The aim of this work is to show how a high-field electron-solid phase in the 2DEG may be detected by optical means in graphene. We have calculated the DOS and the LDOS of electron-solid phases in the Hartree-Fock approximation in the $N=2$ LL.

We show that the number of low-energy DOS peaks in graphene is given by the number of electrons per site M_e. This result is similar to the previous DOS calculation in the Hartree-Fock approximation for GaAs.[9]

We found that the rescaled LDOS is identical for different filling factors ν_N, as long as the ratio ν_N/M_e, which determines the lattice spacing of the M_e-electron bubble crystal, is kept fixed, and the LDOS frequency is taken at the DOS peak with the same index (for the first four indices). In particular, this result yields an unexpected conclusion that, e.g., by fixing the filling factor $\nu_N=0.14$ in the $N=2$ LL and using STM, one could observe in the LDOS the whole succession of electron-crystal density patterns with $M_e=1$, 2, and 3 by fixing the applied STM voltage at the consecutive first three single-particle excitation energies, and summing up the LDOS to obtain the resummed LDOS $\tilde{A}(\mathbf{r},\omega)$.

We believe that this LDOS correspondence holds true for all single-particle excitations resolved as individual DOS peaks so far (accounting for interchanging of the last two peaks in the $M_e=2$ and 3 cases) and for all LLs (similar conclusions follow from our calculations in the LLs $N=1$, 3, and 4). We also obtained the same LDOS correspondence for other models of the 2DEG: (i) in a single-layer GaAs heterostructure; (ii) U(1)-graphene; and (iii) bilayer. This implies that the observed LDOS ν_N/M_e scaling is independent of the underlying interaction potential and the number of inner discrete degrees of freedom. The fact that the U(1)-graphene results coincide numerically with those for graphene indicates that the electron crystals considered here are completely valley-pseudospin polarized.

ACKNOWLEDGMENTS

We thank P. Lederer for fruitful discussions. O.P. acknowledges financial support from the European Commission through the Marie-Curie Foundation under Contract No. MEST CT 2004-51-4307, and from the Gates Cambridge Scholarship Trust. M.O.G. was partially funded by the Agence Nationale de la Recherche under Grants No. ANR-06-NANO-019-03 and No. ANR-JCJC-0003-01. The work of C.M.S. was partially supported by the Netherlands Organization for Scientific Research (NWO).

*apopl@ukr.net, op226@cam.ac.uk

[1] E. Wigner, Phys. Rev. **46**, 1002 (1934).
[2] C. C. Grimes and G. Adams, Phys. Rev. Lett. **42**, 795 (1979).
[3] H. Fukuyama, P. M. Platzman, and P. W. Anderson, Phys. Rev. B **19**, 5211 (1979).
[4] D. Yoshioka and H. Fukuyama, J. Phys. Soc. Jpn. **47**, 394 (1979).
[5] D. Yoshioka and P. A. Lee, Phys. Rev. B **27**, 4986 (1983).
[6] H. Fukuyama and P. A. Lee, Phys. Rev. B **17**, 535 (1978); **18**, 6245 (1978).
[7] A. A. Koulakov, M. M. Fogler, and B. I. Shklovskii, Phys. Rev. Lett. **76**, 499 (1996); M. M. Fogler, A. A. Koulakov, and B. I. Shklovskii, Phys. Rev. B **54**, 1853 (1996); R. Moessner and J. T. Chalker, *ibid.* **54**, 5006 (1996).
[8] M. O. Goerbig, P. Lederer, and C. Morais Smith, Phys. Rev. B **69**, 115327 (2004).
[9] R. Côté, C. B. Doiron, J. Bourassa, and H. A. Fertig, Phys. Rev. B **68**, 155327 (2003).
[10] E. Fradkin and S. A. Kivelson, Phys. Rev. B **59**, 8065 (1999); M. M. Fogler, in *High Magnetic Fields*, edited by C. Berthier, L. P. Lévy, and G. Martinez (Springer-Verlag, Berlin, 2001).
[11] H. L. Stormer, D. C. Tsui, and A. C. Gossard, Rev. Mod. Phys. **71**, S298 (1999).
[12] J. P. Eisenstein, K. B. Cooper, L. N. Pfeiffer, and K. W. West, Phys. Rev. Lett. **88**, 076801 (2002).
[13] K. B. Cooper, M. P. Lilly, J. P. Eisenstein, L. N. Pfeiffer, and K. W. West, Phys. Rev. B **60**, R11285 (1999).
[14] M. O. Goerbig, P. Lederer, and C. Morais Smith, Phys. Rev. B **68**, 241302(R) (2003).
[15] E. Y. Andrei, G. Deville, D. C. Glattli, F. I. B. Williams, E. Paris, and B. Etienne, Phys. Rev. Lett. **60**, 2765 (1988).
[16] H. A. Fertig, in *Perspectives in Quantum Hall Effects*, edited by S. Das Sarma and A. Pinczuk (Wiley, New York, 1997).
[17] F. I. B. Williams, P. A. Wright, R. G. Clark, E. Y. Andrei, G. Deville, D. C. Glattli, O. Probst, B. Etienne, C. Dorin, C. T. Foxon, and J. J. Harris, Phys. Rev. Lett. **66**, 3285 (1991).
[18] R. M. Lewis, P. D. Ye, L. W. Engel, D. C. Tsui, L. N. Pfeiffer, and K. W. West, Phys. Rev. Lett. **89**, 136804 (2002).
[19] R. M. Lewis, Y. Chen, L. W. Engel, D. C. Tsui, P. D. Ye, L. N. Pfeiffer, and K. W. West, Phys. Rev. Lett. **93**, 176808 (2004).
[20] R. M. Lewis, Y. P. Chen, L. W. Engel, D. C. Tsui, L. N. Pfeiffer, and K. W. West, Phys. Rev. B **71**, 081301(R) (2005).
[21] Y. P. Chen, R. M. Lewis, L. W. Engel, D. C. Tsui, P. D. Ye, Z. H. Wang, L. N. Pfeiffer, and K. W. West, Phys. Rev. Lett. **93**, 206805 (2004).
[22] Y. P. Chen, G. Sambandamurthy, Z. H. Wang, R. M. Lewis, L. W. Engel, D. C. Tsui, P. D. Ye, L. N. Pfeiffer, and K. W. West, Nat. Phys. **2**, 452 (2006).
[23] Ø. Fischer, M. Kugler, I. Maggio-Aprile, and C. Berthod, Rev. Mod. Phys. **79**, 353 (2007).
[24] A. K. Geim and K. S. Novoselov, Nature Mater. **6**, 183 (2007).
[25] For a review, see A. H. Castro Neto, F. Guinea, N. M. R. Peres, K. S. Novoselov, and A. K. Geim, Rev. Mod. Phys. **81**, 109 (2009).
[26] K. S. Novoselov, A. K. Geim, S. V. Morozov, D. Jiang, M. I. Katsnelson, I. V. Grigorieva, S. V. Dubonos, and A. A. Firsov, Nature (London) **438**, 197 (2005).
[27] Y. Zhang, Y.-W. Tan, H. L. Stormer, and P. Kim, Nature (London) **438**, 201 (2005).
[28] K. S. Novoselov, Z. Jiang, Y. Zhang, S. V. Morozov, H. L. Stormer, U. Zeitler, J. C. Maan, G. S. Boebinger, P. Kim, and A. K. Geim, Science **315**, 1379 (2007).
[29] M. O. Goerbig, R. Moessner, and B. Douçot, Phys. Rev. B **74**, 161407(R) (2006).
[30] V. M. Apalkov and T. Chakraborty, Phys. Rev. Lett. **97**, 126801 (2006).
[31] C. Tőke, P. E. Lammert, V. H. Crespi, and J. K. Jain, Phys. Rev. B **74**, 235417 (2006); C. Tőke and J. K. Jain, *ibid.* **75**, 245440 (2007).
[32] D. V. Khveshchenko, Phys. Rev. B **75**, 153405 (2007).
[33] M. O. Goerbig and N. Regnault, Phys. Rev. B **75**, 241405(R) (2007); R. de Gail, N. Regnault, and M. O. Goerbig, *ibid.* **77**, 165310 (2008).
[34] For a recent review on a possible fractional quantum Hall effect, see Z. Papić, M. O. Goerbig, and N. Regnault, Solid State Commun. **149**, 1056 (2009).
[35] C.-H. Zhang and Yogesh N. Joglekar, Phys. Rev. B **75**, 245414 (2007).
[36] C.-H. Zhang and Yogesh N. Joglekar, Phys. Rev. B **77**, 205426 (2008).
[37] J. Wang, A. Iyengar, H. A. Fertig, and L. Brey, Phys. Rev. B **78**, 165416 (2008).
[38] H. Wang, D. N. Sheng, L. Sheng, and F. D. M. Haldane, Phys. Rev. Lett. **100**, 116802 (2008).
[39] R. Côté, J.-F. Jobidon, and H. A. Fertig, Phys. Rev. B **78**, 085309 (2008).
[40] J. Martin, N. Akerman, G. Ulbricht, T. Lohmann, J. H. Smet, K. von Klitzing, and A. Yacoby, Nat. Phys. **4**, 144 (2008).
[41] P. Mallet, F. Varchon, C. Naud, L. Magaud, C. Berger, and J.-Y. Veuillen, Phys. Rev. B **76**, 041403(R) (2007).
[42] G. Li, A. Luican, and E. Y. Andrei, Phys. Rev. Lett. **102**, 176804 (2009).
[43] H. P. Dahal, Y. N. Joglekar, K. S. Bedell, and A. V. Balatsky, Phys. Rev. B **74**, 233405 (2006).
[44] R. Côté and A. H. MacDonald, Phys. Rev. Lett. **65**, 2662 (1990); Phys. Rev. B **44**, 8759 (1991).
[45] R. Côté, L. Brey, and A. H. MacDonald, Phys. Rev. B **46**, 10239 (1992).
[46] K. Nomura and A. H. MacDonald, Phys. Rev. Lett. **96**, 256602 (2006).
[47] J. Alicea and M. P. A. Fisher, Phys. Rev. B **74**, 075422 (2006).
[48] G. D. Mahan, *Many-Particle Physics* (Indiana University, Bloomington, 1980).
[49] P. K. Lam and S. M. Girvin, Phys. Rev. B **30**, 473 (1984); **31**, 613(E) (1985).